ISSN 0915-6364

NATIONAL INSTITUTE FOR FUSION SCIENCE

Dynamical Simulation for Sputtering of B_4C

T. Kenmotsu, T. Kawamura, T. Ono and Y. Yamamura

(Received - Feb. 4, 1998)

NIFS-DATA-46 Mar. 1998

RESEARCH REPORT
NIFS-DATA Series

NAGOYA, JAPAN

Dynamical Simulation for Sputtering of B_4C

T.Kenmotsu*, T.Kawamura, T.Ono*** and Y.Yamamura*****

**The Graduate University for Advanced Studies*
332-6 Oroshi-cho,Toki-shi,509-5292,Japan
***National Institute for Fusion Science*
332-6 Oroshi-cho,Toki-shi,509-5292,Japan
****Okayama University of Science*
1-1, Ridai-cho,Okayama,700-0005, Japan

Abstract

Using ACAT-DIFFUSE code, we have simulated the fluence dependence of B_4C sputtering and the associated surface composition change under D^+ ion bombardment. The ACAT-DIFFUSE is a simulation code, which is based on a Monte Carlo method with a binary collision approximation and solves diffusion equations. In the case of near–threshold sputtering, the preferential sputtering of B atoms is enhanced by the threshold effect. As a result, the total sputtering yield at the steady-state is reduced by about 20% compared with low-fluence sputtering. The surface concentration at steady-state is determined by the competitive processes between diffusion and surface-atom removal due to sputtering. At normal incidence the interstitial diffusion contributes appreciably to the steady-state surface concentration, but at grazing incidence this effect is small. Therefore, the steady-state surface concentration ratio at grazing incidence is less than that of normal incidence.

Key words: Sputtering, Ion Irradiation, Surface Effects, Metals, Alloys and Compounds, Diffusion

1. Introduction

Plasma-facing components, such as limiters and divertors, receive large fluxes of high energy particles. As a result, the constituent atoms of those materials are sputtered from the surface into the core plasma as impurities. Impurities cause core plasma cooling.

To reduce impurity generation, both low Z and high Z materials are adopted as candidates for plasma-facing components. High flux beam bombardment on B_4C was studied at high temperature [1][2][3]. Those experiments show that the sputtering yield of B_4C (boron carbide) are suppressed compared to that of graphite. This property could give the B_4C material some advantage in the plasma-facing component.

The main concern of this paper is to simulate the fluence dependence of B_4C sputtering and the associated surface composition changes under D^+ ion bombardment at normal and grazing incidences. For this purpose we have applied the ACAT-DIFFUSE [4][5] to light ion sputtering from B_4C.

2. Simulation model

A detailed description of the ACAT-DIFFUSE code has been given elsewhere [4][5]. Only a very brief outline is given here. The code assumes an amorphous target material and it is based on the binary collision approximation. In the code, the total dose Φ is divided into small dose increments $\Delta\Phi$ during which the bombarding ions do not change the target composition appreciably. The ions corresponding to $\Delta\Phi$ are assumed to hit the target material simultaneously and be slowed down instantaneously. Their slowing down, together with the associated vacancy and range distributions are

simulated by the ACAT routine. These collided atoms diffuse during the time interval of $\Delta\Phi/J$ (J being the current density). The diffusion process is estimated by solving the diffusion equations numerically in the DIFFUSE routine. In the code, these procedures are repeated n times, where $n= \Phi/ \Delta\Phi$. The logical representation of the code is ACAT-DIFFUSE = $[(ACAT)(DIFUSE)]^n$.

3. Numerical results and discussions

One of the most important parameters for divertor erosion is the threshold sputtering due to light ions at normal and grazing incidences. A threshold sputtering of 50 eV ion bombardment is considered. We adopted 1.0×10^{18} ions/cm^2/sec as a D^+ current density and the target temperature was set to be 300K. This current density corresponds to the flux received by a divertor plate in a fusion reactor under steady-state operation. We assumed that the interstitial diffusion is dominant at this temperature and we neglect the vacancy diffusion and segregation. The respective acceptable activation energy of the B atom and the C atom are assumed to be 0.59 eV and 0.60 eV for interstitial diffusion [6].

In B_4C, the B atom is sputtered preferentially, because the surface binding energy of the B atom is lower than that of the C atom. The simulated C_B^S/C_C^S ratios at the topmost layer is shown in Fig.1 as a function of fluence at normal incidence, where 50 eV, 80 eV and 200 eV are employed as the incident energies, and C_B^S and C_C^S are the surface concentrations of the B atom and the C atom, respectively. The inset in Fig. 1 shows the energy dependence of the total sputtering yields from the B_4C material bombarded by an early irradiation whose fluence is denoted by Φ_0 in the following discussions. The

fluence Φ_0 does not affect the surface concentration ratio. The total sputtering yields at 50 eV, 80 eV and 200 eV are 4.8×10^{-3}, 1.1×10^{-2} and 1.8×10^{-2}, respectively. The surface concentration ratio reaches a nearly constant steady-state value after a critical fluence denoted by Φ_{st}. The critical fluences at 50 eV, 80 eV and 200 eV are, approximately, 6.0×10^{17}, 1.6×10^{17} and 1.0×10^{17} ions/cm^2, which correspond to the removal of one surface layer due to sputtering.

The threshold energies of the B atom and the C atom for D^+ ion bombardment at normal incidence are 21.1 eV and 27.2 eV, respectively [7]. For low energies such as 50 eV D^+ the threshold effect enhances the preferential sputtering of B atoms. The relative sputtering yields, Y_B/Y_C, from the B_4C material bombarded at Φ_0 are 9.7, 5.7 and 4.7, respectively, for 50 eV, 80 eV and 200 eV. This is why the steady-state surface concentration ratio of 50 eV is lowest. Thus, the steady-state surface concentration ratio depends on the preferentiality of the sputtering.

Figure 2 shows the surface concentration ratios C_B^S/C_C^S at normal and grazing incidence for 50 eV and 200 eV, where the angle of incidence, θ, is measured from the surface normal. The grazing angles are 65° and 75° for 50 eV and 200 eV, respectively. The normalized sputtering yield, $Y(\theta)/Y(0^\circ)$, is shown in the inset of Fig. 2 as a function of the incident angle θ. $Y(65^\circ)/Y(0^\circ)$ for 50 eV and $Y(75^\circ)/Y(0^\circ)$ for 200 eV are 2.9 and 8.1, respectively, and the relative sputtering yields Y_B/Y_C for grazing incidence are 7.2 and 4.7, respectively, for 50 eV and 200 eV at $\Phi=\Phi_0$.

When the ions are bombarded at grazing incidences, the energy deposition takes place only near the topmost layer and few interstitial atoms are produced in a deeper layers. This means that the contribution of the diffusion seems to be very small.

Therefore, the stationary surface concentrations are achieved only by the sputtering process and so the stationary values of C_B^S/C_C^S at grazing incidences is lower than that of normal incidence, even if the preferentiality of sputtering at the grazing incidence is less than that of normal incidence. Inversely speaking, the stationary surface concentration at normal incidence is determined by the balance between the interstitial diffusion and the sputtering process.

As is known from Figs. 1 and 2, the surface B concentration at the steady-state is less than that at $\Phi = \Phi_0$ for every case. This means that the total sputtering yields at $\Phi = \Phi_{st}$ are smaller than that at $\Phi = \Phi_0$; this is clearly shown in Table 1. Especially for a 50 eV ion bombardment, the sputtering yields are reduced by more than 20% at the steady-state.

Figure 3 shows the energy distributions of sputtered B and C atoms for 50 eV $D^+ \rightarrow B_4C$ under various bombarding conditions. In the case of light ion sputtering, almost all sputtered atoms are primary kicked-off recoil atoms due to reflected light ions, not due to the collision cascade. This is why the high energy tails of the energy spectra drop sharply compared with the Thompson formula [8].

The possible maximum energy of a sputtered atom at normal and grazing incidences will be roughly estimated by $(1 - \gamma)\gamma E$ and γE, respectively, where γ is the elastic energy transfer factor. The γE's of sputtered B and C atoms are 26.46 eV and 24.60 eV, respectively. The $(1 - \gamma)\gamma E$'s of sputtered B and C atoms are 12.46 eV and 12.50 eV, respectively. This is why the high energy edge of sputtered B atoms is larger than that of sputtered C atoms at grazing incidences and why the high energy edge at normal incidence is less than that at grazing incidences.

The difference of the energy spectra between $\Phi = \Phi_0$ and $\Phi = \Phi_{st}$ at grazing incidence is larger than that at normal incidence. This tendency reflects completely the difference in the surface concentration ratios C_B^S/C_C^S between $\Phi = \Phi_0$ and $\Phi = \Phi_{st}$ which is shown in Fig.2.

Figure 4 shows the energy distributions of sputtered B and C atoms for 200 eV $D^+ \rightarrow B_4C$ under various bombarding conditions. The high energy tails of the energy spectra for 200 eV also drop sharply. For 200 eV D^+, the γE's of sputtered B and C atoms are 105.9 eV and 98.4 eV, and the $(1 - \gamma)\gamma E$'s of sputtered B and C atoms are 49.8 eV and 50.0 eV, respectively. Therefore, there are similarities with the energy spectra at 50 eV.

It is well known that sputtered atoms that are ejected after sufficient collision processes will obey the Thompson formula and have a cosine angular distribution. It is interesting that the energy spectra of sputtered C atoms in Figs. 3 and 4 show slightly gentler slopes than those of sputtered B atoms in the higher energy region. Since the C atom density is one-quarter of B atoms in B_4C, an appreciable amount of C atoms will be sputtered by the two-step process, especially for the threshold sputtering such as in the 50 eV ion bombardment. Here, the two-step process means the following: First of all, the B atom with the major concentration is knocked off by the reflected D^+ ion and this knocked-off B atom hits the surface C atom with the minor concentration.

The angular distribution of sputtered atoms is sensitive to the concentration profile near the surface. In the case of the heavy ion sputtering, it shows the strong under-cosine distribution for low energy ion bombardment, and the cosine distribution for high energy ion bombardment. On the contrary, the light ion sputtering always shows the nearly cosine angular distribution, because the light ion sputtering is due to a single

knock-on process. Fig.5 and 6 show the angular distributions of sputtered B and C atoms at normal and grazing incidences for 50 eV D^+ and 200 eV D^+ ions, respectively. Though the angular distributions of C atoms at normal incidence for 50 eV have statistical errors near the surface normal, the angular distributions of both B and C atoms at normal incidence show slightly under-cosine distributions for 50 eV, and nearly cosine distributions for 200 eV. The difference in the angular distributions between $\Phi = \Phi_0$ and $\Phi = \Phi_{st}$ reflects completely the difference of the surface concentration ratios C_B^S/C_C^S between $\Phi = \Phi_0$ and $\Phi = \Phi_{st}$.

The grazing light ion sputtering is mainly due to the direct knock-out process at the topmost surface layer [9]. The effect of two-step process is also observed in the angular distributions of sputtered C atoms of grazing incidence in Fig. 5. The two-step process makes the angular distribution of sputtered atoms broader.

4. Conclusions

Using the ACAT-DIFFUSE code, we simulated sputtering yields of B_4C with near-threshold energy and relatively high energy at normal and grazing incidences. In the case of near-threshold sputtering, the preferential sputtering of B atoms is enhanced by the deference of a threshold energy between the C atom and the B atom, and so the steady-state surface B concentration is much less than the bulk concentration. As a result, the total sputtering yield at the steady-state is reduced by about 20% as compared with low-fluence sputtering. For high energy incidence the fluence effect is not observed appreciably.

The surface concentration at steady-state is determined by the competitive processes

between diffusion and surface recession due to sputtering. At normal incidence there is an appreciable contribution from interstitial diffusion, but for grazing incidence because the energy deposition is limited to near the topmost surface and few interstitial atoms are produced in the deeper layer, the surface concentration is mainly determined by the preferential atom removal.

References

[1] C. Garacia-Rosales, E. Gauthier, J. Roth, R. Schworer and W. Eckstein, J. Nucl. Mater **189** (1992) 1

[2] Y. Ohtuka, M. Isobe, K. Nakano, Y. Ueda, S. Goto, M. Nishikawa, J. Nucl. Mater **222** (1995) 886

[3] M. Isobe, Y. Ohtuka, H. Shinonaga, Y. Ueda, B. Kyoh, M. Nishikawa, Fusion. Eng Des. **28** (1995) 170

[4] Y. Yamamura and T. Kenmotsu, Rad. Eff. Defects. Solids **142** (1997) 385

[5] Y. Yamamura, Nucl. Instr. Meth. B **28** (1987) 17

[6] A. von Oertzen, H.H. Rotermund, S. Nettesheim, Surf. Sci. **311** (1994) 322

[7] Y. Yamamura and J. Bohdansky, Vacuum **35** (1985) 561

[8] G. Falcone and P. Sigmund, Appl.Phys. **25** (1981) 307

[9] Y. Yamamura and N. Itoh, Sputtering Yield, in *Ion Beam Assisted Film Growth*, ed. T. Itoh (Elsevier, Amsterdam), (1989) chap. 4.

Captions of figures and table

Fig. 1. Dose dependence of the C_B^S/C_C^S ratio at the first layer during 50 eV, 80 eV and 200 eV D^+ ion bombardments on B_4C at normal incidence. The inset shows the energy dependence of the total sputtering yield of the B_4C material bombarded by Φ_0 with D^+ ion.

Fig. 2. Dose dependence of the surface concentration ratio C_B^S/C_C^S during 50 eV D^+ and 200 eV D^+ ion bombardments on B_4C at normal and grazing incidences, where the grazing angles are 65° for 50 eV and 75° for 200 eV. The inset shows the normalized sputtering yield, $Y(\theta)/Y(0^\circ)$, as a function of incident angle for 50 eV and 200 eV D^+ ion bombardment on the B_4C material bombarded by Φ_0 with D^+ ion.

Fig. 3. Energy distributions of sputtered B and C atoms from B_4C with 50 eV D^+ ion at normal and grazing incidences at various conditions. The angle of grazing incidence is 65° , and Φ_0 and Φ_{st} refer to low-fluence and the critical fluence, respectively. Symbols mean the ACAT-DIFFUSE data and the solid line mean Thompson formula.

Fig. 4. The same as Fig. 3, but the incident energy is 200 eV and the angle of grazing incidence is 75° .

Fig. 5. Angular distributions of sputtered B and C atoms from B_4C with 50 eV D^+ ion at normal and grazing incidences. The angle of grazing incidence is 65° , and Φ_0 and Φ_{st} are low-fluence and the critical fluence, respectively. (sterad : steradian)

Fig. 6. The same as Fig. 5, but the incident energy is 200 eV and the angle of grazing incidence is 75° .

Table 1 The total sputtering yields at $\Phi = \Phi_{st}$ and $\Phi = \Phi_0$ for 50 eV and 200 eV ion bombardments on B_4C.

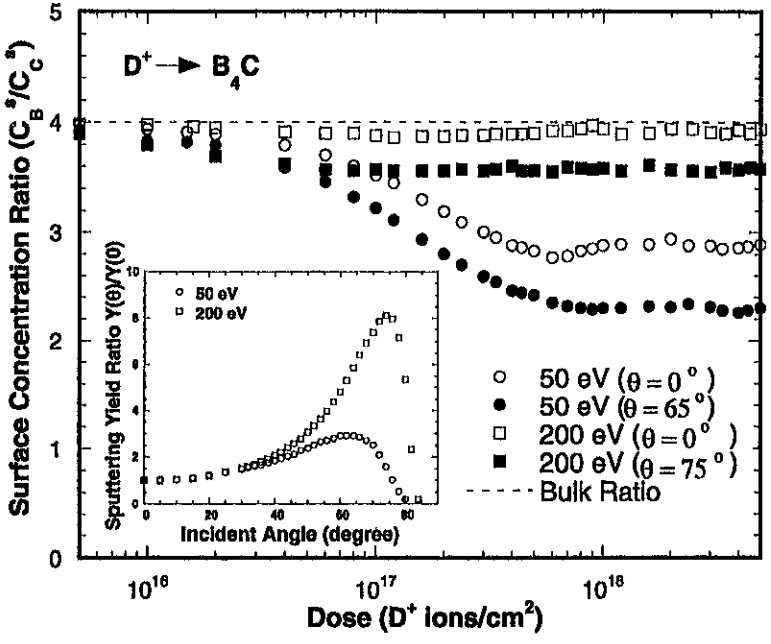
D+ → B4C
Surface Concentration Ratio (CB s/CC s)
Dose (D+ Ions/cm2)
50 eV (θ = 0°)
50 eV (θ = 65°)
200 eV (θ = 0°)
200 eV (θ = 75°)
Bulk Ratio
Sputtering Yield Ratio Y(θ)/Y(0)
Incident Angle (degree)

Fig. 2

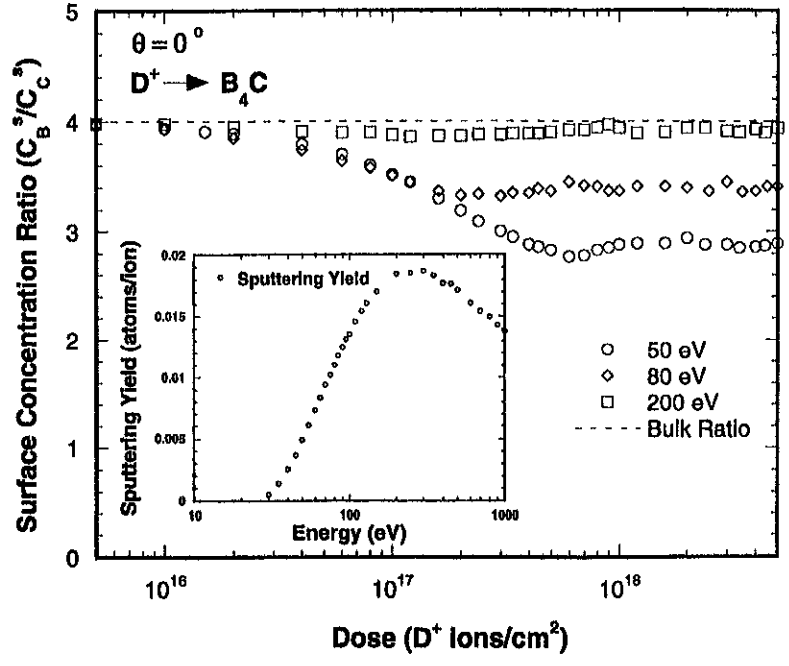
θ = 0°
D+ → B4C
Surface Concentration Ratio (CB s/CC s)
Dose (D+ Ions/cm2)
50 eV
80 eV
200 eV
Bulk Ratio
Sputtering Yield (atoms/ion)
Energy (eV)

Fig. 1

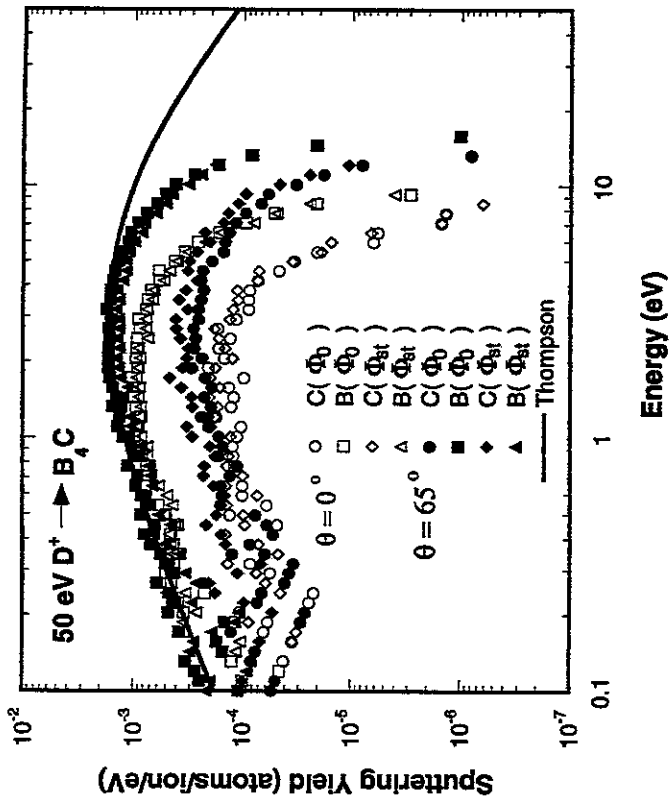
50 eV D+ → B4C
Sputtering Yield (atoms/ion/eV)
Energy (eV)
θ = 0°
θ = 65°
C(Φ0)
B(Φ0)
C(Φst)
B(Φst)
Thompson

Fig. 3

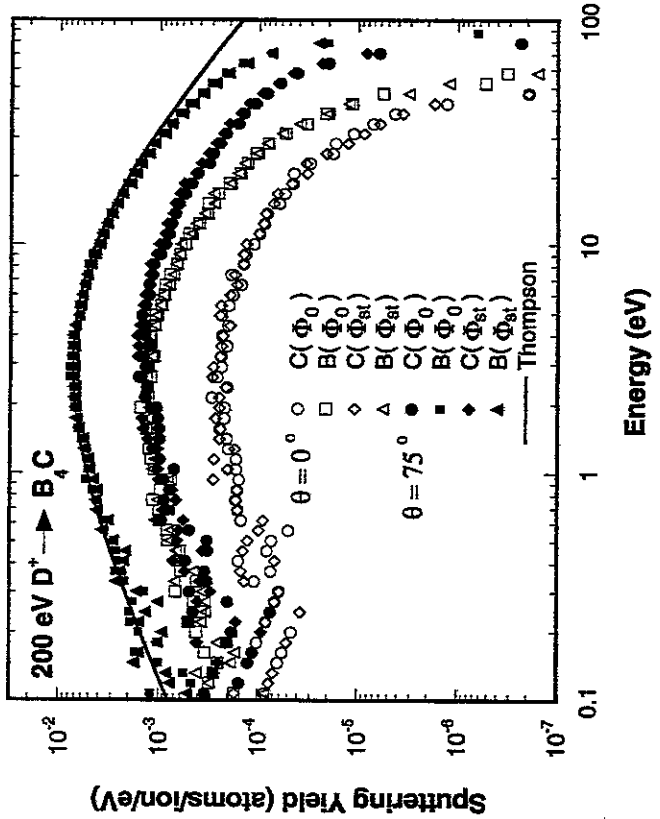
200 eV D+ → B4C
Sputtering Yield (atoms/ion/eV)
Energy (eV)
θ = 0°
θ = 75°
C(Φ0)
B(Φ0)
C(Φst)
B(Φst)
Thompson

Fig. 4

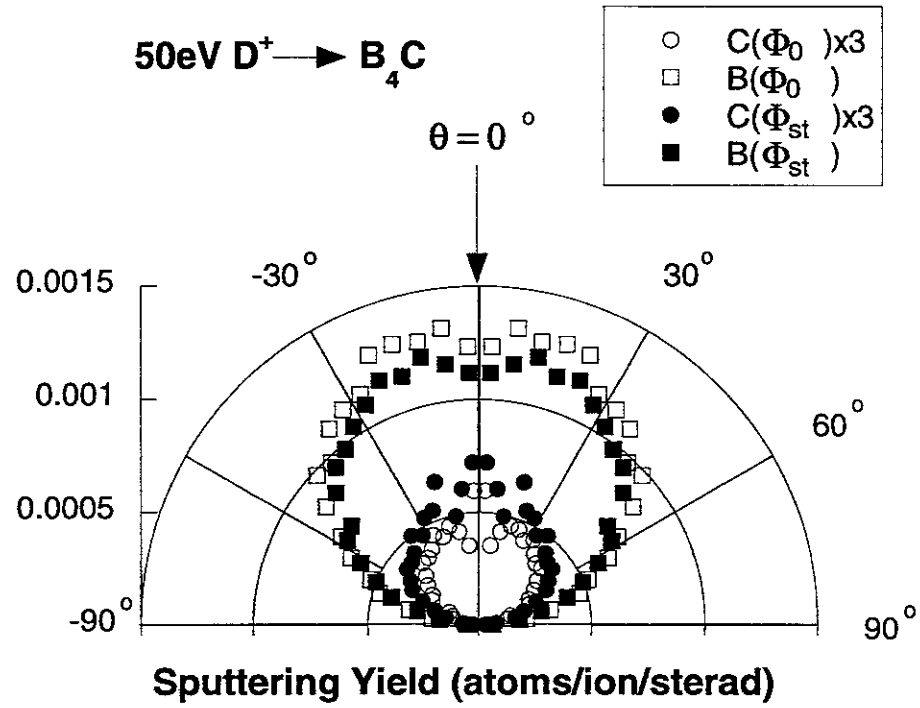
50eV D+ → B4C
C(Φ0)x3
B(Φ0)
C(Φst)x3
B(Φst)
θ = 0 °
-30°
30°
0.0015
0.001
0.0005
60°
-90°
90°
Sputtering Yield (atoms/ion/sterad)

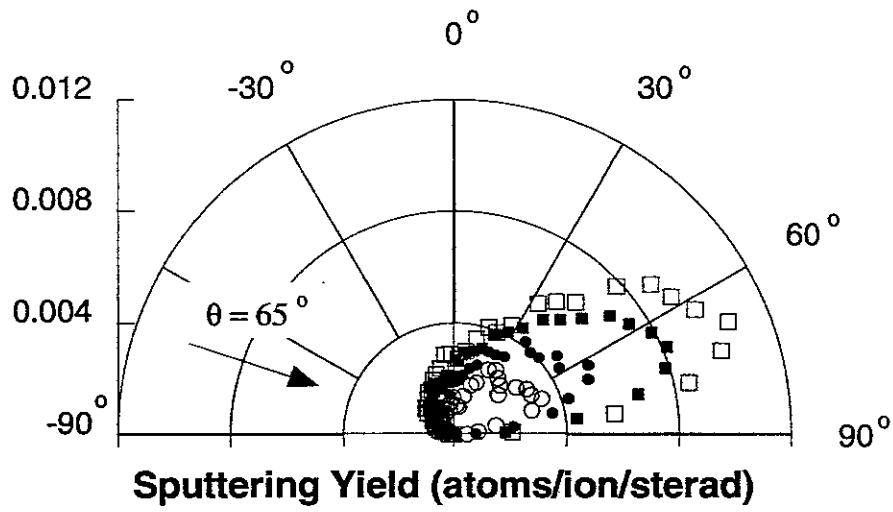
0°
-30°
30°
0.012
0.008
0.004
60°
θ = 65°
-90°
90°
Sputtering Yield (atoms/ion/sterad)

Fig.5

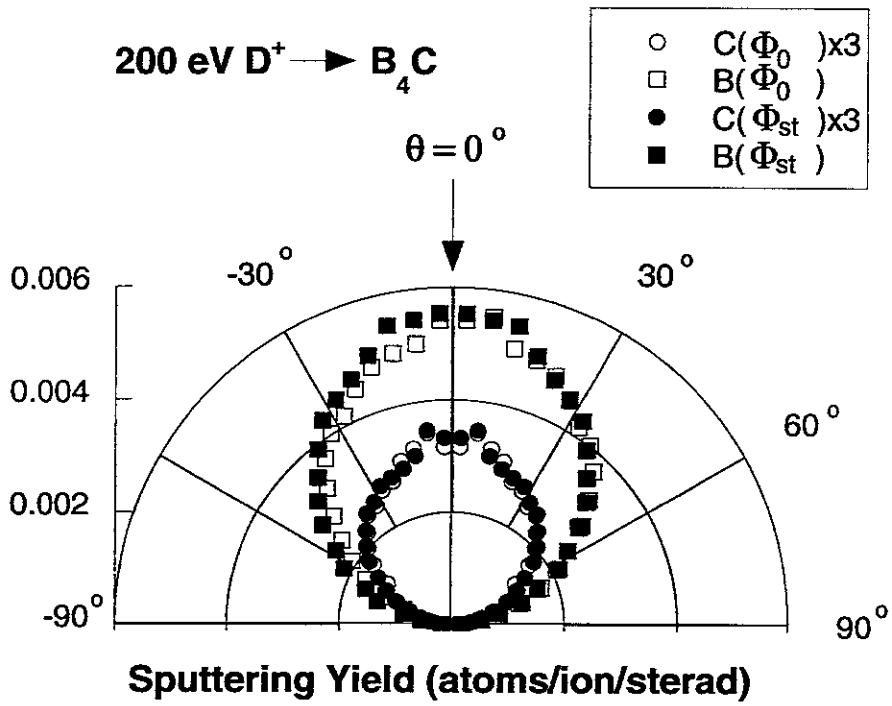
200 eV D+ → B4C
C(Φ0)x3
B(Φ0)
C(Φst)x3
B(Φst)
θ = 0°
-30°
30°
60°
90°
-90°
0.006
0.004
0.002
Sputtering Yield (atoms/ion/sterad)

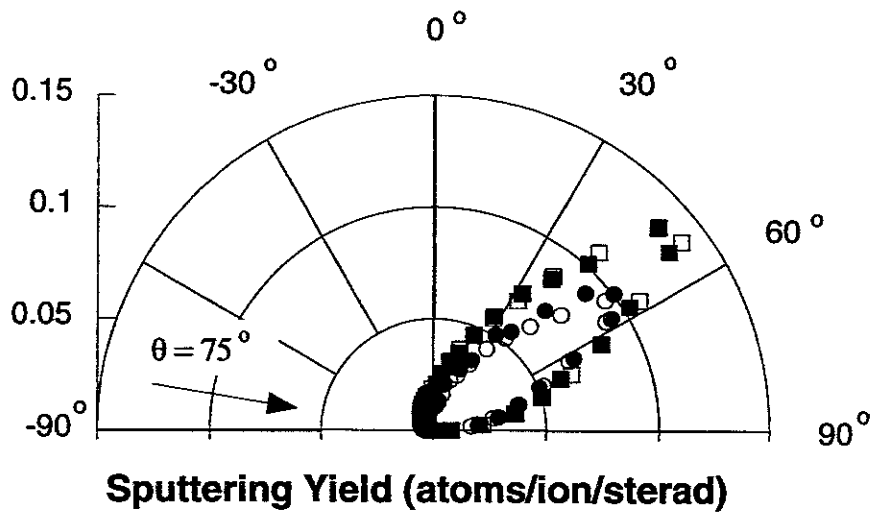
0°
-30°
30°
60°
90°
-90°
θ = 75°
0.15
0.1
0.05
Sputtering Yield (atoms/ion/sterad)

Fig. 6

Table 1

Incident Energy(eV)	θ	Φ_0	Φ_{st}
50	0°	4.8×10^{-3}	4.2×10^{-3}
200	0°	1.8×10^{-2}	1.7×10^{-2}
50	65°	1.5×10^{-2}	1.2×10^{-2}
200	75°	1.5×10^{-1}	1.4×10^{-1}

(atoms/ion)

Recent Issues of NIFS-DATA Series

NIFS-DATA-12 Hiro Tawara,
Total and Partial Cross Sections of Electron Transfer Processes for Be^{q+} and B^{q+} Ions in Collisions with H, H_2 and He Gas Targets -Status in 1991-; June 1991

NIFS-DATA-13 T. Kaneko, M. Nishikori, N. Yamato, T. Fukushima, T. Fujikawa, S. Fujita, K. Miki, Y. Mitsunobu, K. Yasuhara, H. Yoshida and Hiro Tawara,
Partial and Total Electronic Stopping Cross Sections of Atoms for a Singly Charged Helium Ion : Part II; Aug. 1991

NIFS-DATA-14 T. Kato, K. Masai and M. Arnaud,
Comparison of Ionization Rate Coefficients of Ions from Hydrogen through Nickel ; Sep. 1991

NIFS-DATA-15 T. Kato, Y. Itikawa and K. Sakimoto,
Compilation of Excitation Cross Sections for He Atoms by Electron Impact; Mar. 1992

NIFS-DATA-16 T. Fujimoto, F Koike, K. Sakimoto, R Okasaka, K. Kawasaki, K. Takiyama, T. Oda and T. Kato,
Atomic Processes Relevant to Polarization Plasma Spectroscopy ; Apr. 1992

NIFS-DATA-17 H. Tawara,
Electron Stripping Cross Sections for Light Impurity Ions in Colliding with Atomic Hydrogens Relevant to Fusion Research; Apr. 1992

NIFS-DATA-18 T. Kato,
Electron Impact Excitation Cross Sections and Effective Collision Strengths of N Atom and N-Like Ions -A Review of Available Data and Recommendations- ; Sep. 1992

NIFS-DATA-19 Hiro Tawara,
Atomic and Molecular Data for H_2O, CO & CO_2 Relevant to Edge Plasma Impurities, Oct. 1992

NIFS-DATA-20 Hiro. Tawara,
Bibliography on Electron Transfer Processes in Ion-Ion/Atom/Molecule Collisions -Updated 1993-; Apr. 1993

NIFS-DATA-21 J. Dubau and T. Kato,
Dielectronic Recombination Rate Coefficients to the Excited States of C I from C II; Aug. 1994

NIFS-DATA-22 T. Kawamura, T. Ono, Y. Yamamura,
Simulation Calculations of Physical Sputtering and Reflection Coefficient of Plasma-Irradiated Carbon Surface; Aug. 1994

NIFS-DATA-23 Y. Yamamura and H. Tawara,
Energy Dependence of Ion-Induced Sputtering Yields from Monoatomic Solids at Normal Incidence; Mar. 1995

NIFS-DATA-24 T. Kato, U. Safronova, A. Shlyaptseva, M. Cornille, J. Dubau,
Comparison of the Satellite Lines of H-like and He-like Spectra; Apr. 1995

NIFS-DATA-25 H. Tawara,
Roles of Atomic and Molecular Processes in Fusion Plasma Researches - from the cradle (plasma production) to the grave (after-burning) -; May 1995

NIFS-DATA-26 N. Toshima and H. Tawara
Excitation, Ionization, and Electron Capture Cross Sections of Atomic Hydrogen in Collisions with Multiply Charged Ions; July 1995

NIFS-DATA-27 V.P. Shevelko, H. Tawara and E.Salzborn,
Multiple-Ionization Cross Sections of Atoms and Positive Ions by Electron Impact; July 1995

NIFS-DATA-28 V.P. Shevelko and H. Tawara,
Cross Sections for Electron-Impact Induced Transitions Between Excited States in He: n, n'=2,3 and 4; Aug. 1995

NIFS-DATA-29 U.I. Safronova, M.S. Safronova and T. Kato,
Cross Sections and Rate Coefficients for Excitation of Δn = 1 Transitions in Li-like Ions with 6<Z<42; Sep. 1995

NIFS-DATA-30 T. Nishikawa, T. Kawachi, K. Nishihara and T. Fujimoto,
Recommended Atomic Data for Collisional-Radiative Model of Li-like Ions and Gain Calculation for Li-like Al Ions in the Recombining Plasma; Sep. 1995

NIFS-DATA-31 Y. Yamamura, K. Sakaoka and H. Tawara,
Computer Simulation and Data Compilation of Sputtering Yield by Hydrogen Isotopes ($^1H^+$, $^2D^+$, $^3T^+$) and Helium ($^4He^+$) Ion Impact from Monatomic Solids at Normal Incidence; Oct. 1995

NIFS-DATA-32 T. Kato, U. Safronova and M. Ohira,
Dielectronic Recombination Rate Coefficients to the Excited States of CII from CIII; Feb. 1996

NIFS-DATA-33 K.J. Snowdon and H. Tawara,
Low Energy Molecule-Surface Interaction Processes of Relevance to Next-Generation Fusion Devices; Mar. 1996

NIFS-DATA-34 T. Ono, T. Kawamura, K. Ishii and Y. Yamamura,
Sputtering Yield Formula for B_4C Irradiated with Monoenergetic Ions at Normal Incidence; Apr. 1996

NIFS-DATA-35 I. Murakami, T. Kato and J. Dubau,
UV and X-Ray Spectral Lines of Be-Like Fe Ion for Plasma Diagnostics; Apr. 1996

NIFS-DATA-36 K. Moribayashi and T. Kato,
Dielectronic Recombination of Be-like Fe Ion; Apr. 1996

NIFS-DATA-37 U. Safronova, T. Kato and M. Ohira,
Dielectronic Recombination Rate Coefficients to the Excited States of CIII from CIV; July 1996

NIFS-DATA-38 T. Fujimoto, H. Sahara, G. Csanak and S. Grabbe,
Atomic States and Collisional Relaxation in Plasma Polarization Spectroscopy: Axially Symmetric Case; Oct. 1996

NIFS-DATA-39 H. Tawara (Ed.)
Present Status on Atomic and Molecular Data Relevant to Fusion Plasma Diagnostics and Modeling; Jan. 1997

NIFS-DATA-40 Inga Yu. Tolstikhina,
LS-Averaged 1/Z Method as a Tool of Studying the Interactions of Highly Charged Ions with a Metal Surface; Jan. 1997

NIFS-DATA-41 K. Moribayashi and T. Kato,
Atomic Nuclear Charge Scaling for Dielectronic Recombination to Be-like Ions; Apr. 1997

NIFS-DATA-42 H. Tawara,
Bibliography on Electron Transfer Processes in Ion-ion / Atom / Molecule Collisions -Updated 1997 -; May 1997

NIFS-DATA-43 M. Goto and T. Fujimoto,
Collisional-radiative Model for Neutral Helium in Plasma: Excitation Cross Section and Singlet-triplet Wavefunction Mixing; Oct. 1997

NIFS-DATA-44 J. Dubau, T. Kato and U.I. Safronova,
Dielectronic Recombination Rate Coefficients to the Excited States of CI From CII; Jan. 1998

NIFS-DATA-45 Y. Yamamura, W. Takeuchi and T. Kawamura,
The Screening Length of Interatomic Potential in Atomic Collisions; Mar. 1998

NIFS-DATA-46 T. Kenmotsu, T. Kawamura, T. Ono and Y. Yamamura,
Dynamical Simulation for Sputtering of B4C; Mar. 1998